PROCEEDINGS OF SCIENCE

Interpretation of the CALET Electron+Positron Spectrum by Astrophysical Sources

Holger Motz[a,*] **for the CALET collaboration**

[a] *Kanagawa University, 3-27-1 Rokkakubashi, Kanagawa, Yokohama, Kanagawa 221-8686, Japan*

E-mail: motz@aoni.waseda.jp

The ISS-based Calorimetric Electron Telescope (CALET) is directly measuring the energy spectrum of electron+positron cosmic rays up to 20 TeV. Supernova remnants (SNR) are the most likely astrophysical sources to provide the majority of the electron flux, out of which a few nearby young SNR like Vela are expected to dominate in the TeV-region with potentially detectable spectral signatures. Another expected contribution to the spectrum is from pulsars as a primary positron-electron pair source for explanation of the positron excess. Complementary to the CALET all-electron spectrum, the positron-only spectrum measured by the magnet spectrometer AMS-02 below the TeV range provides detailed information on this component. An interpretation of the CALET and AMS-02 data by overlapping spectra from individual pulsar and SNR point sources is presented, combining sources known from electromagnetic wave observations with further randomly generated ones spread throughout the Galaxy. Based on the study of a large number of samples with randomized source locations and emission spectra parameters, best fitting ranges and constraints for these parameters, as well as predictions for the spectrum beyond the so far measured energy range have been derived.

38th International Cosmic Ray Conference (ICRC2023)
26 July - 3 August, 2023
Nagoya, Japan

ICRC2023
38th International Cosmic Ray Conference
The Astroparticle Physics Conference

*Speaker

PoS(ICRC2023)067

1. Introduction

The bulk of cosmic rays is commonly assumed to originate from shock-wave acceleration in supernova remnants (SNR), based on the measured and predicted power law nature of the spectra with a source spectrum index (before propagation) around 2 and the matching energy of a few supernovae per century and 10^{51} erg per supernova being able to provide the power to maintain the cosmic ray population within the Galaxy, if the energy conversion into cosmic rays is on the order of percent. The flux of electron cosmic rays is about one order of magnitude lower than that of protons, putting the expected efficiency in the order of per-mill and the expected energy emitted per supernova in electron cosmic rays to 10^{48} erg [1]. Compared to nuclei, electrons experience stronger energy loss through synchrotron radiation and inverse Compton scattering during propagation, limiting the distance and thus number of sources that can contribute to the spectrum at high energy, down to only a few in the TeV region with the Vela SNR expected to dominate [1]. In several publications [2–4], Monte Carlo simulations have been used to ascertain the possibility and assess the probability of SNR and pulsar populations with various properties to be a valid explanation of the measured electron and positron spectra, finding that a small fraction of the randomly generated samples would agree to the data. This work follows the same principles, but is partly motivated by the need to construct an astrophysical base model for indirect dark matter search described in Ref. [5], and therefore introduces a method in which average parameters of the sources are adapted to the data by direct fitting, increasing the rate at which models matching the data are found. The parameters are the source spectrum power-law indices ($\gamma_{i(SNR)}$ and $\gamma_{i(pulsar)}$), cut-off energies ($E_{cut(SNR)}$ and $E_{cut(pulsar)}$), and the efficiencies at which electron cosmic rays are accelerated by the SNRs and pulsars ($\eta_{(SNR)}$ and $\eta_{(pulsar)}$). This study yields the ranges in the space spanned by these parameters in which samples matching the measured data could be found. While the sample density in the parameter space might be a measure of the probability of these parameters occurring, it is at best a qualitative measure as the sample construction and fitting introduces biases. The used data-sets are the CALET all-electron flux shown at ICRC2021 [6] over the full energy range from 10.6 GeV to 4.8 TeV, as well as the AMS-02 positron-only flux [7] from 2 GeV to 1 TeV. To estimate possible outcomes of the CALET measurement beyond the current maximum energy, the number of events that would be expected to be measured by CALET above 4.8 TeV was calculated for each sample, assuming a detector livetime of 2×10^8 seconds, 1040 cm^2 effective area and 80% reconstruction efficiency.

2. Random Sample Construction

Each sample of pulsars and SNRs comprises the sources within the Galaxy up to an age of 200 Myr, a time over which all emitted electron and positron cosmic rays are estimated to fall below the lower energy threshold of 2 GeV by radiative energy loss. The spatial distribution of supernovae and associated pulsars in the Galaxy is taken from Ref. [8], with a supernova rate of 2.1 per 100 years, while the rate of pulsar births is set to 1.7 per 100 years following Ref. [9]. Sources with a distance of up to 30 kpc from the solar system are considered, comprising the whole galactic disk. For the kinetic energy of the supernovae, the values of $log_{10}(Q_{SNR}/\mathrm{erg})$ are drawn from a normal distribution with mean 51 and width 1, and a hard cut-off at 5×10^{52} erg.

The initial rotation energy of pulsars, is determined by drawing $log_{10}(Q_{pulsar}/\mathrm{erg})$ from a normal distribution with mean 49.30 and width 1.01, which are obtained from a fit to the energies of the pulsars in the ATNF catalog [10], calculated from age T as $Q_{pulsar} = \dot{Q}\, T^2/\tau$, where $\tau = 10$ kyr is the assumed spin-down timescale [11]. While the emission of the electron cosmic rays from SNR is assumed to be instantaneous at the time of the supernova explosion, the electron-positron pairs from pulsars may be trapped in the pulsar wind nebula for several 10 kyr, therefore a release delay time T_R is subtracted from their age to obtain the injection time T_i. In the construction of each random sample, first the positions, ages and energies of pulsars are generated. To these randomly generated pulsars, those listed in the ATNF catalog are added. For each ATNF catalog pulsar, a randomly generated pulsar falling into the same energy, age and distance bin is removed, if present. The spatial distribution of the sources in one sample is illustrated in Fig. 1.

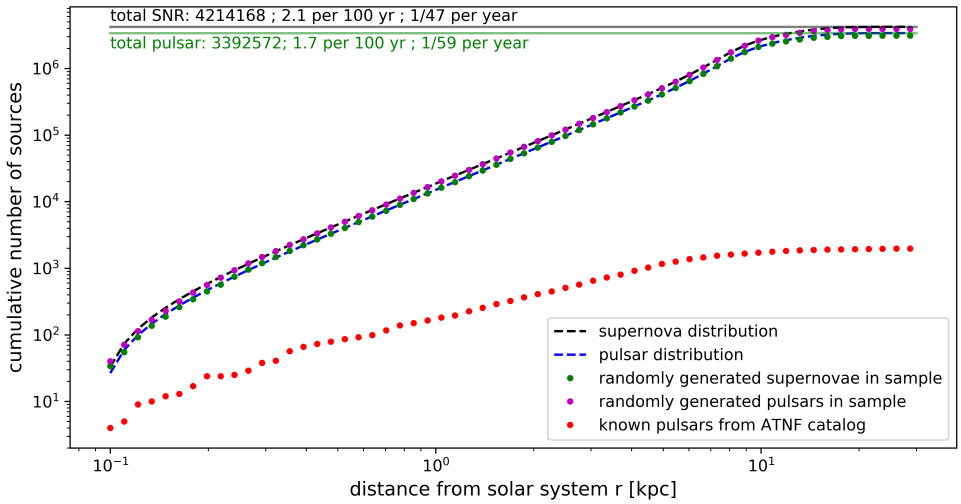

Figure 1: Distribution of astrophysical sources as a function of distance from the solar system for one of the samples. The number of observed pulsars in the ATNF catalog is much smaller than the expected and randomly generated number due to observation bias.

3. Propagation and Local Flux Calculation

The parameters governing propagation are taken from the model explained in Ref. [12], based on matching the output of calculations of the spallation network with DRAGON to the measured nuclei spectra under the assumption that all nuclei species share a common power law with cut-off source spectrum and the structures (hardening, softening) in the observed spectra are due to propagation effects. The flux $\Phi(E)$ from each point source propagated to the solar system is calculated using the semi-analytical method established in ref. [2], expressed in kinetic energy and adapted to the dual break in the diffusion coefficient slope inherent in the propagation model:

$$\Phi(E) = \frac{Q_0 \eta}{\pi^{3/2} r_{dif}^3} E_0^{-\gamma_i} e^{-\frac{E_0}{E_{cut}}} \frac{b(E_0)}{b(E)} e^{-\frac{r^2}{r_{dif}^2}} , \qquad (1)$$

where r is the distance between source and the solar system, E_0 is the electron energy at emission obtained by resolving $t_i(E, E_0) = \int_E^{E_0} \frac{1}{b(E')} dE'$ for it and the characteristic diffusion distance $r_{dif} = \sqrt{\int_E^{E_0} \frac{D(E')}{b(E')} dE'}$ and the energy loss coefficient $b(E) = b_{IC}(E) + b_{SYN}(E)$ is dependent on energy, comprising the inverse Compton loss term $b_{IC}(E)$ including Klein-Nishina effect and the synchrotron loss term $b_{SYN}(E)$, defined as in ref. [2]. The diffusion coefficient is defined as:

$$D(E) = D_{0(@sol)} \left(\frac{E}{E_0}\right)^{\delta_l} \left(1 + \left(\frac{E}{E_{bl}}\right)^{\frac{\delta_l - \delta}{s}}\right)^{s} \left(1 + \left(\frac{E}{E_{bh}}\right)^{\frac{\delta - \delta_h}{s}}\right)^{-s} . \tag{2}$$

The integrals and energy loss terms are solved beforehand and look-up tables for $E_0(E, t_i)$ and $r_{dif}(E, E_0)$ prepared to speed up the calculation process. Still, the calculation of the spectra of over 7 million sources by this method takes too much computation time to use it as the input function of a minimization algorithm. To remedy this, the parameters are treated as follows:

- The combined flux from all pulsars or SNRs is pre-calculated and tabulated for several values of the power law index. In the fitting, the flux for any index γ_i is retrieved from the fluxes for higher and lower indices γ_h and γ_l by the following interpolation:

$$\Phi(\gamma_i) = \frac{\gamma_h - \gamma_i}{\gamma_h - \gamma_l} \Phi(\gamma_l) \left(\frac{E}{GeV}\right)^{\gamma_l - \gamma_i} + \frac{\gamma_i - \gamma_l}{\gamma_h - \gamma_l} \Phi(\gamma_h) \left(\frac{E}{GeV}\right)^{\gamma_h - \gamma_i} \tag{3}$$

- The cut-off energies are scanned, i.e. the fits are performed for discrete values of $E_{cut(SNR)}$ and $E_{cut(pulsar)}$.
- The average acceleration efficiencies $\eta_{(SNR)}$ and $\eta_{(pulsar)}$ are fitted directly, since they represent just a scaling factor for the SNR and pulsar flux.

To the primary astrophysical sources, the fluxes of secondary electrons and positrons are added, which are taken from the DRAGON nuclei spectra calculations used to define the propagation model [12]. Solar modulation is treated by the force-field approximation with an energy and charge-sign dependent potential inspired by Ref. [13] given by

$$\Phi(R) = \Phi_0 + \Phi_{1\pm} \frac{1 + (R/R_r)^2}{(R/R_r)^3} , \tag{4}$$

introducing the base potential Φ_0, the additional potentials Φ_{1+} and Φ_{1-} for positively and negatively charged particles respectively, as well as the reference rigidity R_r as additional fit parameters. For CALET data, the energy dependent 1σ deviation $\Delta(E)$ is calculated for each data point in the same way as the values listed in the supplemental material of Ref. [14] for the following systematic uncertainty sources: Normalization, tracking, charge selection, electron identification, Monte Carlo model dependence. A shift by $w\Delta(E)$ is performed as part of the fit function with the weight w for each systematic uncertainty source as a free parameter and each squared weight added to the total χ^2 of the fit as explained in Ref. [15]. Taking the correlation of the systematic uncertainties over the whole energy range into account in this way ensures that the smoothness of the measured spectrum is better represented in the fitting than if using quadratic addition of statistical and systematic errors. Systematic errors without known energy dependence (trigger and BDT proton rejection) are added quadratically to the statistical error.

4. Fitting and Parameter Spread Procedure

In the first step, all pulsars and all SNRs are assumed to have the same source spectrum index and the same acceleration efficiency, respectively. To obtain an initial estimate of these parameters, fitting to AMS-02 data and to CALET data is performed separately. The positron flux is solely determined by the parameters of the pulsars, with $\gamma_{i(pulsar)}$ and $\eta_{(pulsar)}$ fitted directly, while $E_{cut(pulsar)}$ and R_T are scanned in the ranges from 1 to 10 TeV and 0 to 60 kyr, respectively. With the pulsar parameters and thus their flux contribution fixed, the CALET data is fitted, optimizing $\gamma_{i(SNR)}$ and $\eta_{(SNR)}$ with a scan over $E_{cut(SNR)}$ in the range from 10 to 100 TeV. In the next step, a random spread with Gaussian distribution is applied to γ_i and $log_{10}(\eta)$ of the individual pulsars and SNRs in the sample, with widths of 0.033 and 0.33 respectively. The distributions are cut off at 3σ, allowing for a maximum deviation from the mean of 0.1 in the index and one order of magnitude in efficiency. This randomization is repeated together with fitting the averages to the data, first for pulsars (AMS-02), then for SNRs (CALET), taking the random sample with lowest χ^2 from 1000 attempts each, or the first for which $\chi^2/ndof < 1$. Finally, combined fits of AMS-02 and CALET data are performed, while scanning over $E_{cut(pulsar)}$ and $E_{cut(SNR)}$ on logarithmic scale with 10 values per decade. The scan is repeated by extending it by one decade in each parameter from the previous best fit position, until no better fit is found. From this mapping of fit quality and fit parameters in the $E_{cut(pulsar)} - E_{cut(SNR)}$ plane, the best fit locations in the parameter space are extracted and shown in Fig. 3 as colored dots for those samples which give a good fit to the data, which is defined as $\chi^2/ndof < 1$ for the combined data-set and $\chi^2 < 1\sigma$-threshold for both of AMS-02 and CALET data-sets. To find the 85 shown well fitting samples, 251 samples were initially created, showing that this model fits the data with high probability if adjusting the average parameters by fitting. The fitted fluxes of two samples are shown in Fig. 2, illustrating the composition of the spectra by the most contributing individual sources and secondary components, as well as the wide range of the event numbers that could be expected to be measured in CALET above 4.8 TeV. All locations where the fit quality is within the 1σ bound are collected over all samples and smoothed with a Gaussian kernel density estimate (KDE) function to create the favored region contours also presented in Fig. 3. No hard exclusion of a parameter space can be derived from this information, however the region in the $E_{cut(pulsar)} - E_{cut(SNR)}$ plane which was scanned, but in which χ^2 of all samples was found to be above the 90%CL threshold, could be considered disfavored. It is also shown in Fig. 3 as a KDE contour.

5. Interpretation

- The SNR source spectrum index covers a range of approximately 2 to 3, showing a strong correlation with the acceleration efficiency. A majority of samples clusters around $\eta_{(SNR)} = 5{\times}10^{-4}$, corresponding to an energy of $5{\times}10^{47}$ erg emitted in electron cosmic rays, supporting the initial hypothesis of about 10^{48} erg in electron cosmic rays per SNR and falling well within the energy budget.

- The pulsar source spectrum index is found to be generally harder, covering a range of about 1.4 to 2.5, showing also a strong correlation with the acceleration efficiency. $\eta_{(pulsar)}$ is found to be in the range of a few 10^{-5}, which is a realistic value for the acceleration efficiency.

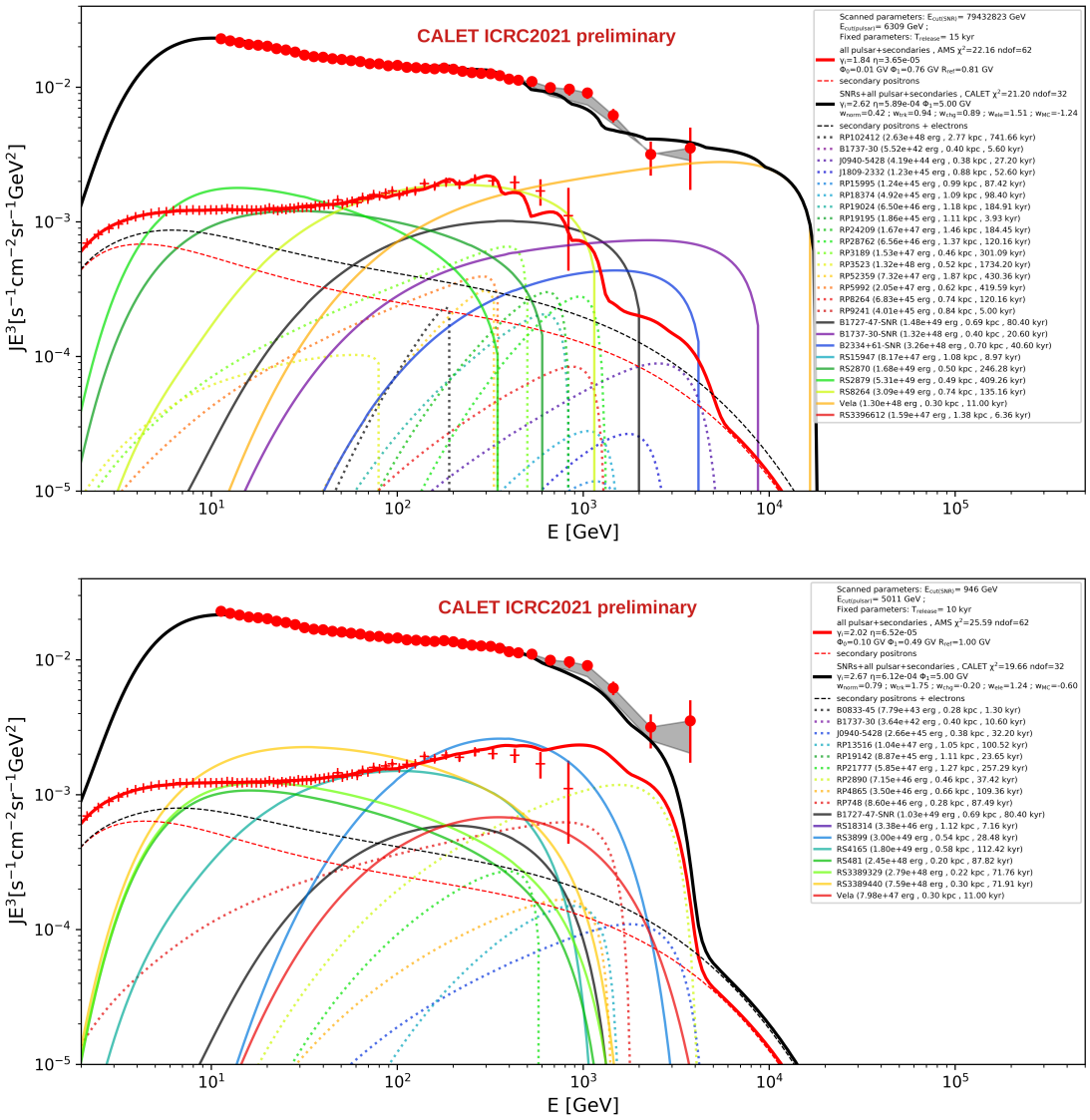

Figure 2: Fit for two of the samples with the contributions of individual astrophysical sources contributing more than 5% to the flux at any energy shown. Details and parameter values in the legend. RP, RS denote randomly generated sources, others are known sources from the ATNF catalog. The upper panel shows a sample with 9.4 events expected in CALET above 4.8 TeV, which the highest among the samples giving a good fit. For the sample in the lower panel, 0.04 events would be expected, showing the wide range of possibilities for the outcome of the CALET measurement in the TeV region.

- The pulsar cut-off energy covers a range of a few hundred GeV to around 100 TeV, with the best-fit cases between several hundred GeV and a few tens of TeV. The SNR cut-off energy on the other hand reaches from several hundred GeV to values of 10^{10} GeV. Such high cut-off values may not be realistic based on the magnetic confinement requirement in the acceleration region, but they indicate that the current electron and positron cosmic ray data provides no constraint on this parameter. However, the sampling indicates that the unbounded SNR cut-

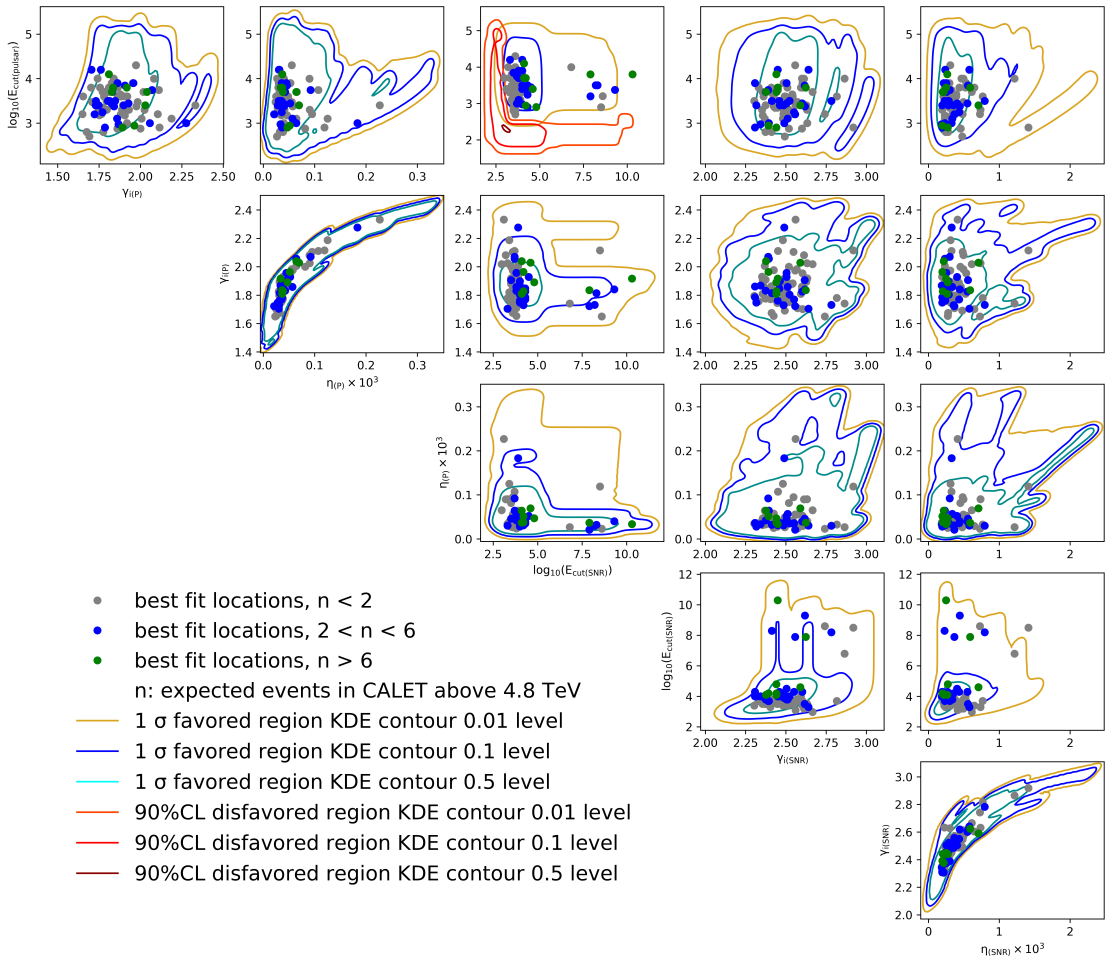

Figure 3: Parameter space covered by the well fitting models. Colored dots represent the best-fit locations, also indicating the prediction for events in CALET above 4.8 TeV. Gold-blue-cyan contours show the regions and sample density (by Gaussian kernel density estimation) where $\chi^2 < 1\ \sigma$-threshold, and red contours show the region where $\chi^2 > 90\%CL$-threshold ($E_{cut(pulsar)} - E_{cut(SNR)}$ plane only).

off requires the source index to be softer than 2.3, which may be understood from a harder index spectra cut-off only by energy loss creating spiky structures not compatible with the smoothness of the measurement.

- The number of events in CALET above 4.8 TeV predicted by the well fitting samples covers a wide range up 9.4 events in case of a significant contribution of Vela in the TeV region. As shown, a very hard drop around a few TeV would be also supported by the data, resulting in a lower number of events than expected from a smooth continuation of the below-TeV spectrum, all the way down to zero expected events above 4.8 TeV. While no obvious correlation with other parameters is found, there is a correlation with the SNR source spectrum cut-off energy, with a low cut-off precluding a high event number. However, no sensitivity beyond 20 TeV is expected since the cut-off from energy loss for the 0.3 kpc distant and 11 kyr old Vela SNR is around this value as shown in Fig. 2. It should be noted that higher energies could be reached

for the Vela spectrum if the emission is not instantaneous, but stretched over a longer period or delayed [16].

6. Conclusion

The CALET all-electron and the AMS-02 positron-only flux measurements can be fit well by the overlapping spectra of randomly generated SNR and pulsar populations, if adjusting the average source spectrum parameters to the data by fitting, with the found fit parameters agreeing with common assumptions on the electron-positron cosmic ray origin. Future extensions of the CALET spectrum to higher energy may provide important information, as the current predictions for the above 4.8 TeV range leave a wide range of potential outcomes, with up to 9.4 events to be detected in CALET (though even higher event numbers might be expected in case of a continuous or delayed release of the cosmic rays from Vela [16]).

Acknowledgments

We gratefully acknowledge JAXA's contributions to the development of CALET and to the operations onboard the International Space Station. The CALET effort in Italy is supported by ASI under Agreement No. 2013-018-R.0 and its amendments. The CALET effort in the United States is supported by NASA through Grants No. 80NSSC20K0397, No. 80NSSC20K0399, and No. NNH18ZDA001N-APRA18-0004. In Japan, this work is supported in part by JSPS Grant-in-Aid for Scientific Research (S) Grant No. 19H05608 and by JSPS Grant-in-Aid for Scientific Research (C) Grant No. JP21H05463.

References

[1] T. Kobayashi, Y. Komori, K. Yoshida, J. Nishimura, *Astrophys. J.* **601**, 340 (2004).
[2] K. Asano, *et al.*, *Astrophys. J.* **926**, 5 (2022).
[3] L. Orusa, S. Manconi, F. Donato, M. D. Mauro, *J. Phys. Conf. Ser.* **2156**, 012086 (2021).
[4] I. Cholis, T. Karwal, M. Kamionkowski, *Phys. Rev. D* **98**, 063008 (2018).
[5] H. Motz, *PoS* **ICRC2023**, 1385 (2023).
[6] S. Torii, Y. Akaike, *PoS* **ICRC2021**, 105 (2021).
[7] M. Aguilar, *et al.*, *Phys. Rev. Lett.* **122**, 041102 (2019).
[8] K. M. Ferrière, *Rev. Mod. Phys.* **73**, 1031 (2001).
[9] K. P. Watters, R. W. Romani, *Astrophys. J.* **727**, 123 (2011).
[10] R. N. Manchester, G. B. Hobbs, A. Teoh, M. Hobbs, *Astron.J.* **129**, 1993 (2005).
[11] J. Feng, H.-H. Zhang, *Eur. Phys. J. C* **76**, 229 (2016).
[12] H. Motz, *PoS* **ICRC2023**, 068 (2023).
[13] I. Cholis, D. Hooper, T. Linden, *Phys. Rev. D* **93**, 043016 (2016).
[14] O. Adriani, *et al.*, *Phys. Rev. Lett.* **120**, 261102 (2018).
[15] H. Motz, Y. Asaoka, S. Bhattacharyya, *PoS* **ICRC2019**, 533 (2019).
[16] H. Motz, *PoS* **ICRC2021**, 100 (2021).

Full Author List: CALET Collaboration

O. Adriani[1,2], Y. Akaike[3,4], K. Asano[5], Y. Asaoka[5], E. Berti[2,6], G. Bigongiari[7,8], W.R. Binns[9], M. Bongi[1,2], P. Brogi[7,8], A. Bruno[10], N. Cannady[11,12,13], G. Castellini[6], C. Checchia[7,8], M.L. Cherry[14], G. Collazuol[15,16], G.A. de Nolfo[10], K. Ebisawa[17], A.W. Ficklin[14], H. Fuke[17], S. Gonzi[1,2,6], T.G. Guzik[14], T. Hams[11], K. Hibino[18], M. Ichimura[19], K. Ioka[20], W. Ishizaki[5], M.H. Israel[9],9 K. Kasahara[21], J. Kataoka[22], R. Kataoka[23], Y. Katayose[24], C. Kato[25], N. Kawanaka[20], Y. Kawakubo[14], K. Kobayashi[3,4], K. Kohri[26], H.S. Krawczynski[9], J.F. Krizmanic[12], P. Maestro[7,8], P.S. Marrocchesi[7,8], A.M. Messineo[8,27], J.W. Mitchell[12], S. Miyake[28], A.A. Moiseev[29,12,13], M. Mori[30], N. Mori[2], H.M. Motz[18], K. Munakata[25], S. Nakahira[17], J. Nishimura[17], S. Okuno[18], J.F. Ormes[31], S. Ozawa[32], L. Pacini[2,6], P. Papini[2], B.F. Rauch[9], S.B. Ricciarini[2,6], K. Sakai[11,12,13], T. Sakamoto[33], M. Sasaki[29,12,13], Y. Shimizu[18], A. Shiomi[34], P. Spillantini[1], F. Stolzi[7,8], S. Sugita[33], A. Sulaj[7,8], M. Takita[5], T. Tamura[18], T. Terasawa[5], S. Torii[3], Y. Tsunesada[35,36], Y. Uchihori[37], E. Vannuccini[2], J.P. Wefel[14], K. Yamaoka[38], S. Yanagita[39], A. Yoshida[33], K. Yoshida[21], and W.V. Zober[9]

[1]Department of Physics, University of Florence, Via Sansone, 1 - 50019, Sesto Fiorentino, Italy, [2]INFN Sezione di Firenze, Via Sansone, 1 - 50019, Sesto Fiorentino, Italy, [3]Waseda Research Institute for Science and Engineering, Waseda University, 17 Kikuicho, Shinjuku, Tokyo 162-0044, Japan, [4]JEM Utilization Center, Human Spaceflight Technology Directorate, Japan Aerospace Exploration Agency, 2-1-1 Sengen, Tsukuba, Ibaraki 305-8505, Japan, [5]Institute for Cosmic Ray Research, The University of Tokyo, 5-1-5 Kashiwa-no-Ha, Kashiwa, Chiba 277-8582, Japan, [6]Institute of Applied Physics (IFAC), National Research Council (CNR), Via Madonna del Piano, 10, 50019, Sesto Fiorentino, Italy, [7]Department of Physical Sciences, Earth and Environment, University of Siena, via Roma 56, 53100 Siena, Italy, [8]INFN Sezione di Pisa, Polo Fibonacci, Largo B. Pontecorvo, 3 - 56127 Pisa, Italy, [9]Department of Physics and McDonnell Center for the Space Sciences, Washington University, One Brookings Drive, St. Louis, Missouri 63130-4899, USA, [10]Heliospheric Physics Laboratory, NASA/GSFC, Greenbelt, Maryland 20771, USA, [11]Center for Space Sciences and Technology, University of Maryland, Baltimore County, 1000 Hilltop Circle, Baltimore, Maryland 21250, USA, [12]Astroparticle Physics Laboratory, NASA/GSFC, Greenbelt, Maryland 20771, USA, [13]Center for Research and Exploration in Space Sciences and Technology, NASA/GSFC, Greenbelt, Maryland 20771, USA, [14]Department of Physics and Astronomy, Louisiana State University, 202 Nicholson Hall, Baton Rouge, Louisiana 70803, USA, [15]Department of Physics and Astronomy, University of Padova, Via Marzolo, 8, 35131 Padova, Italy, [16]INFN Sezione di Padova, Via Marzolo, 8, 35131 Padova, Italy, [17]Institute of Space and Astronautical Science, Japan Aerospace Exploration Agency, 3-1-1 Yoshinodai, Chuo, Sagamihara, Kanagawa 252-5210, Japan, [18]Kanagawa University, 3-27-1 Rokkakubashi, Kanagawa, Yokohama, Kanagawa 221-8686, Japan, [19]Faculty of Science and Technology, Graduate School of Science and Technology, Hirosaki University, 3, Bunkyo, Hirosaki, Aomori 036-8561, Japan, [20]Yukawa Institute for Theoretical Physics, Kyoto University, Kitashirakawa Oiwake-cho, Sakyo-ku, Kyoto, 606-8502, Japan, [21]Department of Electronic Information Systems, Shibaura Institute of Technology, 307 Fukasaku, Minuma, Saitama 337-8570, Japan, [22]School of Advanced Science and Engineering, Waseda University, 3-4-1 Okubo, Shinjuku, Tokyo 169-8555, Japan, [23]National Institute of Polar Research, 10-3, Midori-cho, Tachikawa, Tokyo 190-8518, Japan, [24]Faculty of Engineering, Division of Intelligent Systems Engineering, Yokohama National University, 79-5 Tokiwadai, Hodogaya, Yokohama 240-8501, Japan, [25]Faculty of Science, Shinshu University, 3-1-1 Asahi, Matsumoto, Nagano 390-8621, Japan, [26]Institute of Particle and Nuclear Studies, High Energy Accelerator Research Organization, 1-1 Oho, Tsukuba, Ibaraki, 305-0801, Japan, [27]University of Pisa, Polo Fibonacci, Largo B. Pontecorvo, 3 - 56127 Pisa, Italy, [28]Department of Electrical and Electronic Systems Engineering, National Institute of Technology (KOSEN), Ibaraki College, 866 Nakane, Hitachinaka, Ibaraki 312-8508, Japan, [29]Department of Astronomy, University of Maryland, College Park, Maryland 20742, USA, [30]Department of Physical Sciences, College of Science and Engineering, Ritsumeikan University, Shiga 525-8577, Japan, [31]Department of Physics and Astronomy, University of Denver, Physics Building, Room 211, 2112 East Wesley Avenue, Denver, Colorado 80208-6900, USA, [32]Quantum ICT Advanced Development Center, National Institute of Information and Communications Technology, 4-2-1 Nukui-Kitamachi, Koganei, Tokyo 184-8795, Japan, [33]College of Science and Engineering, Department of Physics and Mathematics, Aoyama Gakuin University, 5-10-1 Fuchinobe, Chuo, Sagamihara, Kanagawa 252-5258, Japan, [34]College of Industrial Technology, Nihon University, 1-2-1 Izumi, Narashino, Chiba 275-8575, Japan, [35]Graduate School of Science, Osaka Metropolitan University, Sugimoto, Sumiyoshi, Osaka 558-8585, Japan, [36]Nambu Yoichiro Institute for Theoretical and Experimental Physics, Osaka Metropolitan University, Sugimoto, Sumiyoshi, Osaka 558-8585, Japan, [37]National Institutes for Quantum and Radiation Science and Technology, 4-9-1 Anagawa, Inage, Chiba 263-8555, Japan, [38]Nagoya University, Furo, Chikusa, Nagoya 464-8601, Japan, [39]College of Science, Ibaraki University, 2-1-1 Bunkyo, Mito, Ibaraki 310-8512, Japan

PoS(ICRC2023)067